

Rocky coastal cliffs reinforced by vegetation roots and potential collapse risk caused by sea-level rise

Tetsuya Kogure

Institute of Environmental Systems Science, Shimane University, 1060 Nishikawatsu-cho, Matsue, Shimane 690-8504, Japan

ARTICLE INFO

Keywords:

Rocky coastal cliff
Stability analysis
Pandanus odoratissimus
Vegetation roots
Reinforcement
Sea-level rise

ABSTRACT

Evaluation of the effect of vegetation roots on the stability of rocky coastal cliffs is necessary to understand geomorphological, environmental and ecological changes in coastlines caused by sea-level rise (SLR). To better understand these topics, coastal cliffs with and without vegetation were investigated. Study cliffs were selected on Taketomi-jima Island and Kuro-shima Island, both in Okinawa, southwestern Japan, because their environmental settings are similar except for the vegetation cover: the islands are only 10 km away from each other and comprise uplifted coral limestone, with an elevation below 5 m. *Pandanus odoratissimus* (PO) covers the seaward edge of the top surface of the coastal cliffs in Taketomi-jima but is absent in Kuro-shima. Field investigations were conducted on both islands to map the distribution of blocks with the dimension of one side exceeding 1 m to obtain the parameters required for stability analysis. The results indicate that the actual coastal cliff elevation is higher in Taketomi-jima than that in Kuro-shima by approximately 1 m, which results in the presence of PO on the seaward edge of the coastal cliffs in Taketomi-jima and its absence in Kuro-shima. The PO root system likely reinforces the cliffs in Taketomi-jima because the stability analysis results revealed that these cliffs are unstable in terms of their dimensions. Therefore, the possible disappearance of PO in Taketomi-jima caused by an SLR of 1 m in the following several decades or hundred years can increase the apparent frequency of cliff collapses by approximately tenfold.

1. Introduction

Sea-level rise (SLR) caused by global warming has steadily proceeded, accelerating from 1.2 ± 0.2 mm/yr from 1901 to 1990 to 3.0 ± 0.7 mm/yr from 1993 to 2010 (Hay et al., 2015). SLR is accompanied by coastal erosion, especially along sandy beaches (e.g. Bruun, 1962; Leatherman et al., 2000; Zhang et al., 2004; Luijendijk et al., 2018). In addition to sandy beaches, rocky coasts constitute a major component of global coastlines because rocky coasts and sandy beaches occupy approximately 52% (Young and Carilli, 2019) and 31% (Luijendijk et al., 2018), respectively, of global coastlines. Sandy beach erosion related to SLR will increase in the future, as estimated in many studies. However, little is known regarding possible changes in the frequency of rocky coast erosion. This might occur because rocky coasts are recognized to remain almost stable because of the hardness of rocks.

Rocky coast erosion is, in many cases, achieved by cliff recession, which is a consequence of individual cliff collapse. Coastal cliff collapses are classified into four types: flows, topples, slides and falls (Sunamura, 1992). Basal erosion caused by waves typically forms a notch, and this

mechanism is common among all collapse types except for flows. In regard to topples (e.g. Davies et al., 1991; Williams et al., 1993; Matsukura, 2001; Kogure et al., 2006), slides (e.g. Hutchinson, 1972) and falls (e.g. Letortu et al., 2019). Kogure et al. (2006) determined that the critical notch depth to realize toppling failure of the limestone cliffs on the Ryukyu Islands, Japan, ranged from several meters to approximately ten meters. Hutchinson (1972) studied failure of a chalk cliff in Joss Bay, England, and reported that slides occurred when the notch depth reached 50 cm. Letortu et al. (2019) reported that a notch depth of 2.28 m at the cliff foot resulted in chalk cliff instability in Normandy, France. These collapses produced falling blocks or sliding masses with dimensions, such as the height, length and breadth, of approximately 10 m or more. Therefore, a rocky cliff collapse yields a major coastline change over the gradual change due to sandy beach erosion, although the rocky cliff collapse frequency is relatively low.

Artificial structures such as breakwaters and concrete tetrapods are implemented to protect coastlines from erosion. Coastal vegetation, which is tolerant to a high salinity, also effectively protects against erosion (e.g. Mazda et al., 1997; Kathiresan and Rajendran, 2005;

E-mail address: kogure@riko.shimane-u.ac.jp.

<https://doi.org/10.1016/j.catena.2022.106457>

Received 9 July 2021; Accepted 9 June 2022

Available online 23 June 2022

0341-8162/© 2022 The Author(s). Published by Elsevier B.V. This is an open access article under the CC BY license (<http://creativecommons.org/licenses/by/4.0/>).

Tanaka et al., 2007; Alongi, 2008). For example, mangrove forests and *Pandanus* species in the tropics and subtropics are considered natural barriers against coastal erosion. They can dissipate wave energy and retain sediments on beaches even during tsunamis (Kathiresan and Rajendran, 2005; Tanaka et al., 2007; Alongi, 2008). Vegetation can also contribute to slope stability increase through their root systems because the maximum tensile strength of the roots of various vegetation types reaches several hundred megapascals (e.g. De Baets et al., 2008; Genet et al., 2008; Abdi et al., 2010; Burylo et al., 2011; Ji et al., 2012; Vergani et al., 2012; Leung et al., 2015). Therefore, coastal cliffs covered with vegetation can also be reinforced by vegetation roots.

Although coastal vegetation is highly salt and wind tolerant, it may experience moderate to severe salt and wind damage during severe storms and hurricanes (Bezona et al., 2001). These extreme events often result in the death of coastal vegetation and even halophytes such as mangrove species both in the short and long term (e.g. Paling et al., 2008). Considering that SLR will likely contribute to an increased frequency and intensity of the storm surge risk (Walsh et al., 2016), SLR will also result in the disappearance of coastal vegetation along coastlines. Consequently, the disappearance of coastal vegetation will lead to sandy beach erosion and cliff stability reduction.

Evaluation of the effect of vegetation roots on the stability of rocky coastal cliffs is therefore important to understand geomorphological, environmental and ecological changes in coastlines caused by SLR. To better understand these topics, coastal cliffs with and without vegetation were investigated via a stability analysis in this study. The potential collapse risk caused by SLR was also examined.

2. Study sites

The study sites include Taketomi-jima Island and Kuro-shima Island in the southwestern part of the Ryukyu Islands, Okinawa, Japan (Fig. 1). The processes of coastal cliff collapse were investigated in detail through mechanical analysis in Kuro-shima (Kogure and Matsukura, 2010a; 2010b; 2012), whereas a similar analysis was not conducted in Taketomi-jima. Detailed characteristics of the study sites are given below.

2.1. Geomorphological and geological settings.

Taketomi-jima (Fig. 1b) and Kuro-shima (Fig. 1c) are low-lying islands comprising uplifted coral limestone surrounded by fringing reefs located in Sekisei Lagoon (Fig. 2). The Pleistocene coral limestone is referred to as Ryukyu limestone. The top surface of the cliffs on both islands is covered with vegetation, most of which includes *Pandanus odoratissimus* (PO, recently referred to as *Pandanus odorifer* (Callmänder et al., 2021)), a dominant coastal vegetation mainly from South Asia through Polynesia (Fig. 3).

Taketomi-jima is located 4 km away from the southwestern part of Ishigaki-jima (Fig. 1a), with a maximum elevation below 20 m and north-south and east-west widths of 3 and 2 km, respectively (Fig. 1b). The strike and dip of the fault running through the central part of Taketomi-jima is N70°E75°S. Coastal cliffs composed of Ryukyu limestone occur along the island coastline except for the northern part, where sandy beaches dominate. The cliffs exhibit a flat top surface and a particular notch at their base (Fig. 4a). Vertical joints fully transect the

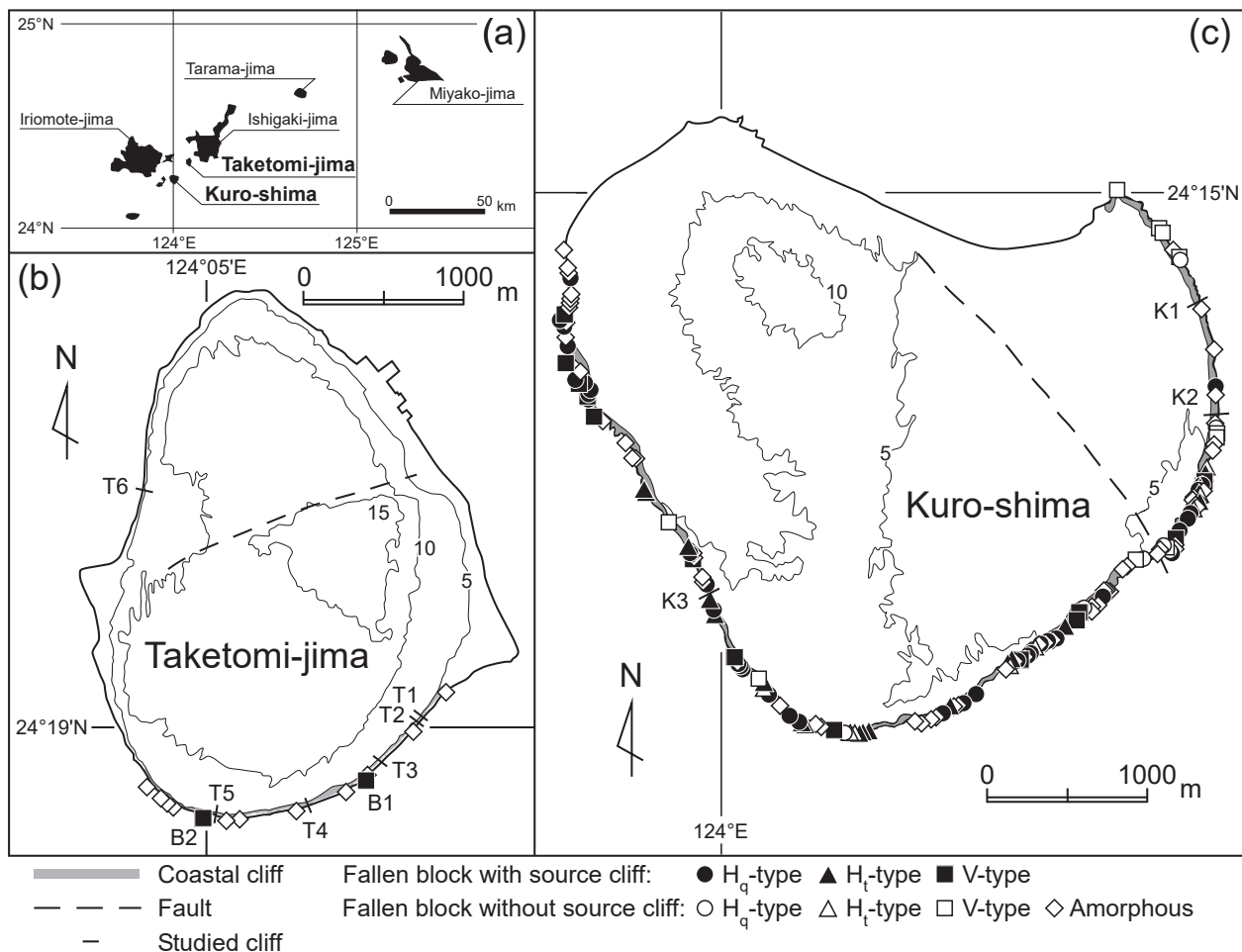


Fig. 1. Locations of the study sites: (a) the southwestern part of the Ryukyu Islands; (b) Taketomi-jima; (c) Kuro-shima.



Fig. 2. Aerial photography of the study sites.

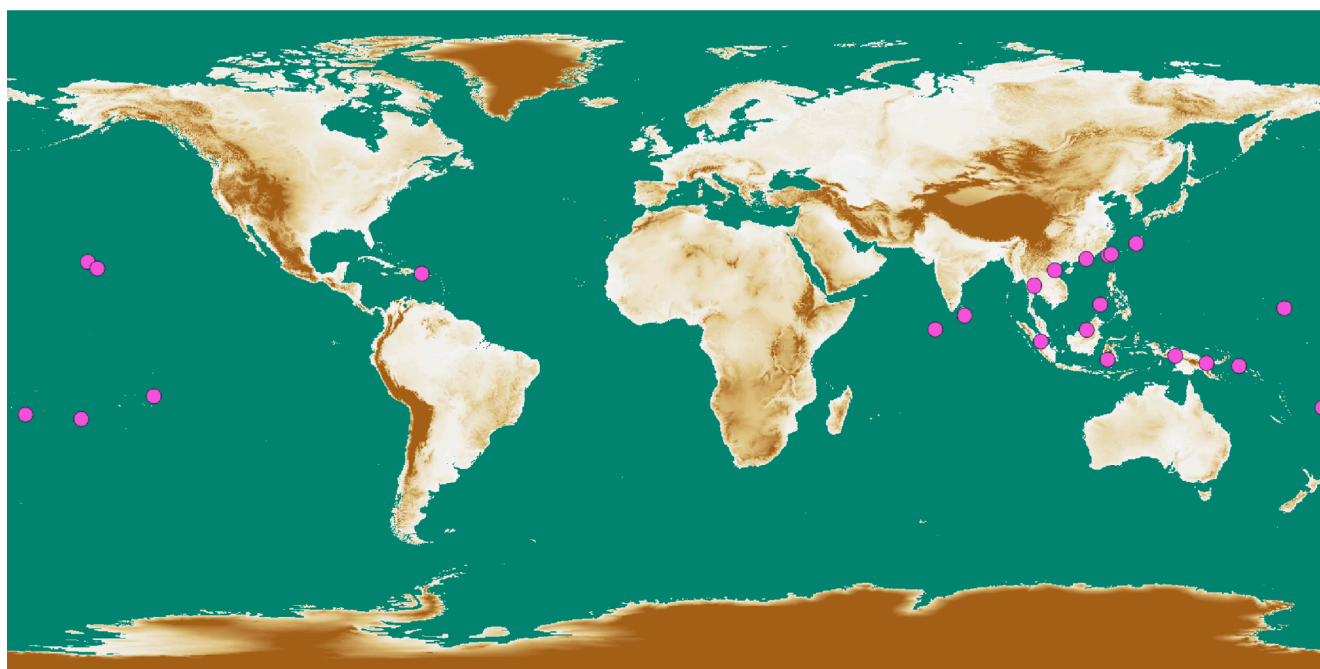


Fig. 3. Distribution map of *Pandanus odoratissimus* worldwide. The data sources include Discover Life (2021) regarding the PO distribution and Geospatial Information Authority of Japan (2021) regarding the global elevation.

cliff and reef flat in front of the cliff (Fig. 4b). The top surface is fully covered with PO (Fig. 4c). The aerial roots of PO with a diameter of ca. 5 cm extend even inside the cliff body to stabilize the top surface, while some roots likely induce cliff collapses by enlarging surface cracks (Fig. 4d).

Kuro-shima is located 10 km away from Taketomi-jima, with a

maximum elevation below 15 m and north–south and east–west widths of 3.5 and 3 km, respectively (Fig. 1c). A low-lying notched cliff with a height ranging from 3 to 4 m occurs along the island coastline from the northeastern part through the south toward the northwestern part (Fig. 1c and 5a). Vertical joints with a crack width between ten and several tens of centimeters are present in coastal cliffs or reef flats



Fig. 4. Coastal cliffs and blocks in Taketomi-jima: (a) top surface of a cliff covered with vegetation; (b) a vertical joint visible on a cliff and reef flats; (c) roots on a cliff surface; (d) a vertical failure surface with roots.

(Fig. 5b). These joints are systematically rather than randomly developed, so they likely originate from geological processes (Kogure and Matsukura, 2011). Vegetation partly covers the flat top surface (Fig. 5a), while no vegetation nor vegetation roots appear on other surfaces, such as notched and failure surfaces (Fig. 5c and 5d, respectively). In contrast to Taketomi-jima, PO does not cover the seaward edge of the top cliff surface in Kuro-shima. PO grows in more inland areas in Kuro-shima, e. g., ca. 50 m from the front face of cliffs (Fig. 6).

Kogure (2009) reported that Ryukyu limestone on both islands exhibits almost the same values of its physical and mechanical properties, such as density, ρ , uniaxial compressive strength, UCS, and tensile strength, S_t (Table 1).

2.2. Cliff collapses

Ryukyu limestone cliff collapses reveal a vertical failure surface (Kogure et al., 2006; Kogure and Matsukura, 2012) or a horizontal failure surface (Kogure and Matsukura, 2010a) (Fig. 7). Kogure et al. (2006) and Kogure and Matsukura (2012) theoretically demonstrated that collapses with a vertical failure surface are induced by the development of tension cracks in the cliff top surface resulting from destabilization by a deepened notch at the cliff base. Kogure and Matsukura (2010a) also theoretically explained the mechanisms of collapses with a horizontal failure surface. The failure body in these cliff collapses is bounded by vertical joints, and therefore, the collapsed cliff is separated from adjacent cliffs by vertical joints before the collapse (Fig. 7). Notch development destabilizes cliffs bounded by vertical joints and finally results in a collapse with a horizontal failure surface, where the failure body collapses into the sea (reef flats). Kogure and Matsukura (2010a) found that the shape of the horizontal failure surface is quadrangular or

triangular, which were denoted as H_q - or H_t -type collapses, respectively (Fig. 7). The shape of the horizontal failure surface changes with the number of vertical joints along coastlines and the intersectional angle between the coastlines and joints (Kogure and Matsukura, 2011). Collapses with a vertical failure surface are referred to as V-type collapses in the present study (Fig. 7).

In addition to Kuro-shima, blocks comprising Ryukyu limestone are found along the Taketomi-jima coastline (Fig. 4). Stability analysis of the blocks occurring in Kuro-shima revealed that many of these blocks were produced by gravity-induced collapses (Kogure and Matsukura, 2010a; Kogure and Matsukura, 2012) or wave-induced collapses of coastal cliffs (Kogure and Matsukura, 2010b; Kogure and Matsukura, 2012). This suggests that the blocks in Taketomi-jima were also likely produced by cliff collapses. Therefore, stability analysis should also be conducted in Taketomi-jima to determine the cliff collapse risk.

3. Methods

3.1. Stability analysis model

Cliffs at risk for H_q - or H_t -type collapses can be identified in advance based on the observation of vertical joints, and instability depends on the development of a notch. In particular, the maximum notch depth is equal to the distance from the front face to the joint surface parallel to the coastline for H_q -type collapse and to the intersection of conjugated joints for H_t -type collapse (L in Fig. 7), whereas the notch depth continues to increase until a collapse occurs for V-type collapse. This allows us to evaluate the stability of H_q - and H_t -type collapses by comparing the critical notch depth calculated with a mechanical equation and the present notch depth observed through field investigation.

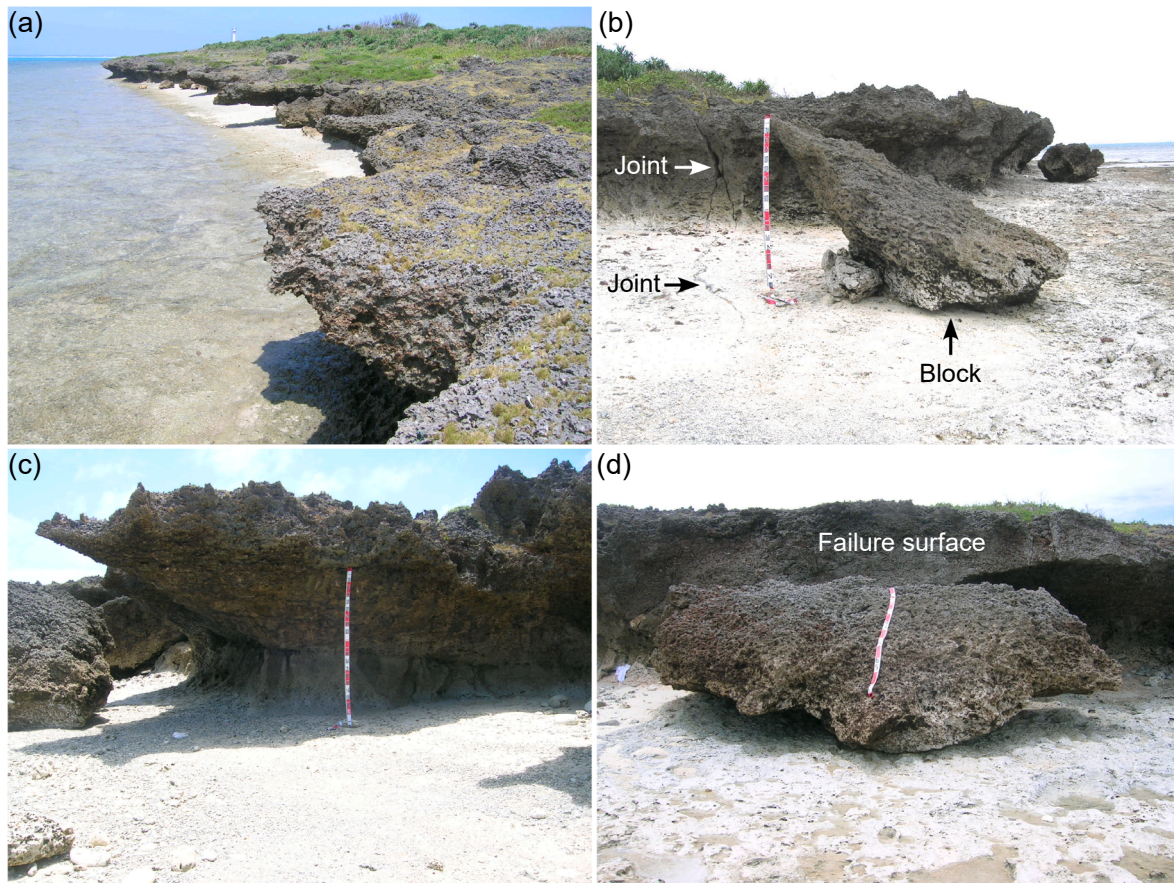


Fig. 5. Coastal cliffs and blocks in Kuro-shima: (a) top surfaces of cliffs covered with less vegetation; (b) vertical joint visible in coastal cliffs and reef flats (modified after Fig. 4a in Kogure and Matsukura (2010a)); (c) notched surface without roots; (d) vertical failure surface without roots.

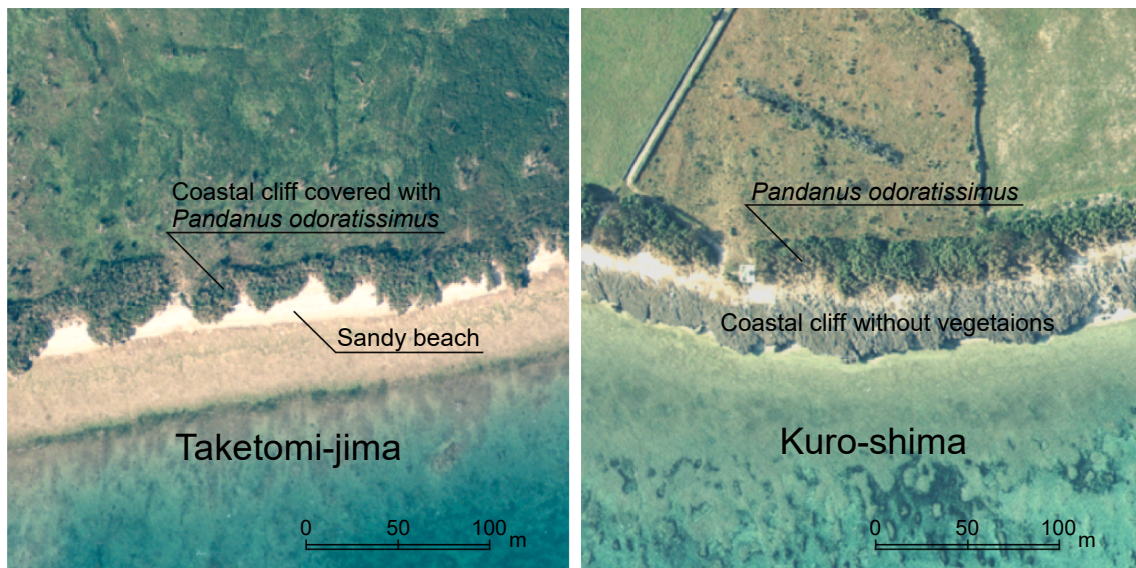


Fig. 6. Difference in vegetation on the top surface of coastal cliffs between Taketomi-jima and Kuro-shima.

The relationship between the stresses acting on a horizontal failure surface and the forces resisting H_q - and H_r -type collapses can be described as follows (Kogure and Matsukura, 2010a):

$$\frac{\beta^2 \rho g (H + 3h)}{(1 - \beta)^2} = \rho g (H + h) + S_t \quad (1)$$

$$\frac{2\beta^2 \rho g}{(1 - \beta)^3} \{2(H + 3h) - \beta(H + 2h)\} = \rho g (H + h) + S_t \quad (2)$$

where H and h denote the height of the notched roof (from the retreat point) and the vertical height of the cliff face, respectively, β is the ratio of the notch depth to the block length, L ($0 \leq \beta < 1$) (Fig. 7) and g is the

Table 1
Physical and mechanical properties of the Ryukyu limestone in Taketomi-jima and Kuro-shima (Kogure, 2009).

Sampling locations	Specimen shape	Size	Number of specimens	Bulk density, Mg/m ³			UCS or S_t , MPa		
				Range	Mean	SD ^a	Range	Mean	SD ^a
<i>Uniaxial compressive strength (UCS)</i>									
Taketomi-jima	Cylinder	Diameter, 35 mm Height, 70 mm	12	2.25–2.36	2.30	0.03	10.6–26.1	21.2	4.3
Kuro-shima	Cylinder	Diameter, 35 mm Height, 70 mm	12	2.23–2.44	2.35	0.06	5.4–37.9	22.1	9.1
<i>Tensile strength (S_t)</i>									
Taketomi-jima	Cylinder	Diameter, 35 mm Height, 35 mm	11	2.14–2.38	2.26	0.08	2.1–7.3	4.2	1.6
Kuro-shima	Cylinder	Diameter, 35 mm Height, 35 mm	12	2.29–2.44	2.37	0.05	3.0–7.3	5.4	1.4

^a Standard deviation.

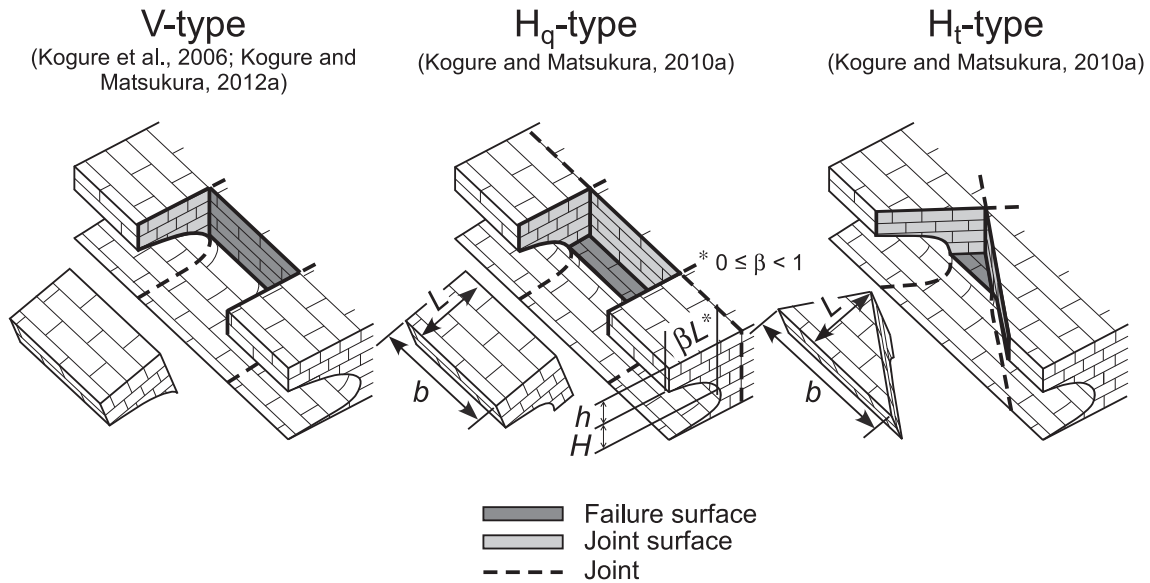


Fig. 7. Types of cliff collapses at the study sites.

gravitational acceleration. The tensile strength, S_t , is given as a function of the length of the potential failure surface by the following equation (Kogure and Matsukura, 2010a):

$$S_t = 1000 \left[5.6 \{ 100(1 - \beta)L \}^{-0.6} + 0.6 \right] \quad (3)$$

The critical value of β for H_q -type collapses, i.e., β_{pred} , can be obtained by substituting Eq. (3) into Eq. (1):

$$\frac{\beta^2 \rho g (H + 3h)}{(1 - \beta)^2} = \rho g (H + h) + 1000 \left[5.6 \{ 100(1 - \beta)L \}^{-0.6} + 0.6 \right] \quad (4)$$

3.2. Field investigation

Field investigations were conducted on both islands to map the distribution of blocks with the dimension of one side exceeding 1 m to determine the parameters required for stability analysis. The block and coastal cliff dimensions (Fig. 7) were measured with a laser range finder and a measuring tape, respectively.

4. Results

4.1. Block and coastal cliff dimensions

Fig. 8 shows vertical profiles of the coastal cliffs on both islands (K2 and K3 were retrieved from Kogure and Matsukura (2012)). The cliff height corresponding to the height from the retreat point of a notch to the top surface, $H + h$, is similar on both islands. However, the elevation of the notch retreat point ranged from 1.87 to 2.53 m in Taketomi-jima and from 0.76 to 1.29 m in Kuro-shima. In addition, the elevation of the

top surface ranged from 3.63 to 4.18 m in Taketomi-jima and from 2.75 to 3.31 m in Kuro-shima. These data indicate that the coastal cliff elevation is approximately 1 m higher in Taketomi-jima than that in Kuro-shima.

Table 2 lists the number of blocks found along the coastline on both islands. The list also includes the number of blocks with a source cliff. In Taketomi-jima, the number of blocks was 13 in total: 5 blocks were identified as being at risk for V-type collapses, and the other blocks were amorphous. Two blocks (B1 and B2, Fig. 1b) out of the five blocks contained a surface corresponding to a failure surface in the cliffs just behind the blocks (Fig. 4d). Consequently, these two blocks were identified as blocks with source cliffs. The original shapes of the amorphous blocks were likely altered through transportation across reef flats caused by large waves during typhoons or severe storms.

In Kuro-shima, 156 blocks were found along the 7.8-km coastline among the coastal cliffs: 24 V-type blocks, 44 H_q -type blocks, 27 H_t -type blocks and 61 amorphous blocks. The number of V-type blocks with a source cliff was 14 (Kogure and Matsukura, 2012) and 35 and 19 for the H_q - and H_t -type blocks, respectively (Kogure and Matsukura, 2010a).

Blocks and remnants of cliff collapses classified as H_q - and H_t -type collapses were not found in Taketomi-jima in the field investigation. However, a few cliffs are at risk for H_q -type collapses because they contain a particular notch at their base and vertical joints aligned for H_q -type collapses (T2, T3 and T5 in Fig. 1b and 9). The top surface of these cliffs is covered with vegetation. In particular, PO dominates T2 and T3. In addition to the observed vertical joints, a horizontal crack is developed at the same elevation as that of the notch retreat point at T3 (Fig. 9b). The crack does not reach the seaward part but branches from vertical joints in the inland part of the cliff, suggesting that the cliff is

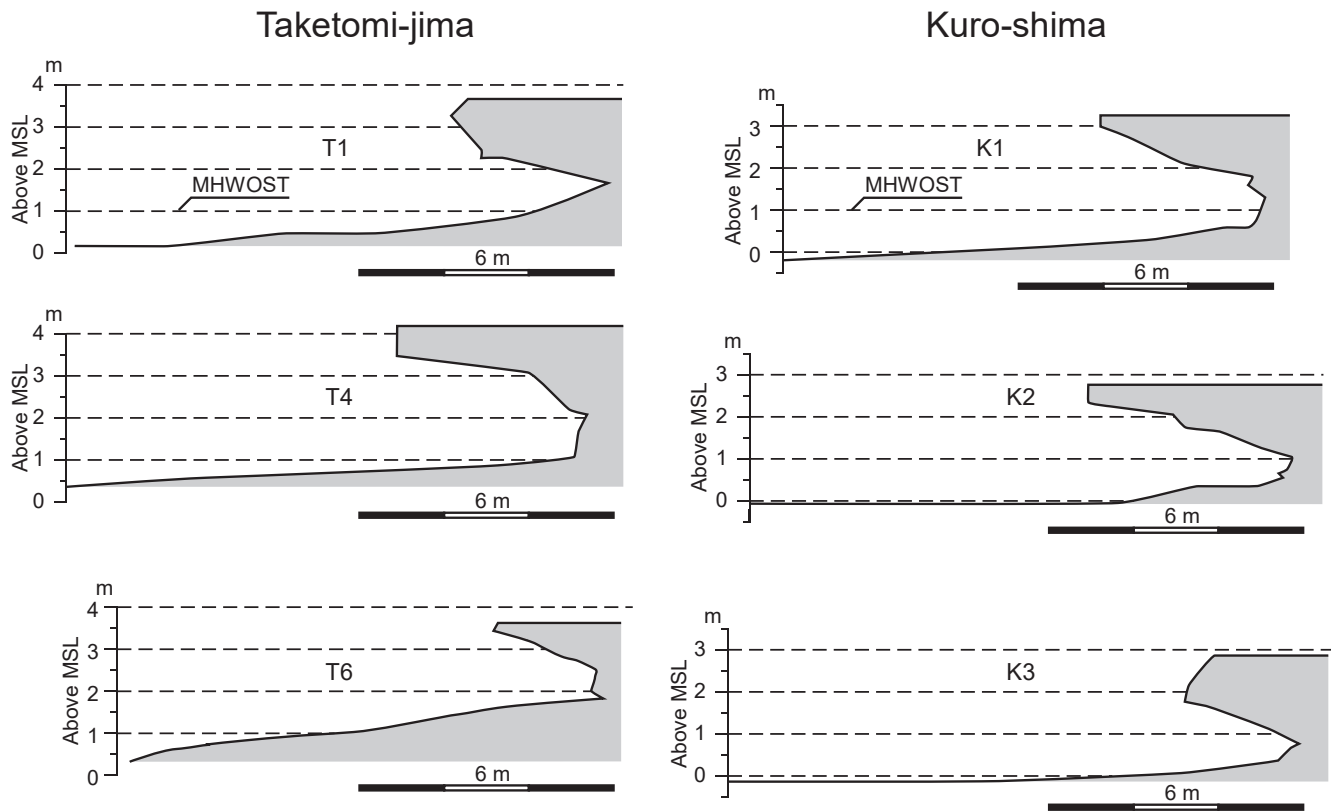


Fig. 8. Vertical profiles of the coastal cliffs in Taketomi-jima and Kuro-shima. MHWOST denotes the mean high water at ordinary spring tide.

Table 2
Number of fallen blocks in Taketomi-jima and Kuro-shima.

Type of fallen block	Total length of rocky coasts (km)	Number of fallen blocks	Number of fallen blocks with source cliff	Frequency of fallen blocks (/km)	Frequency of fallen blocks with source cliff (/km)
<i>Taketomi-jima</i>					
V	–	5	2	1.9	0.8
H _q	–	0	0	0.0	0.0
H _t	–	0	0	0.0	0.0
Amorphous	–	8	0	3.1	0.0
Total	2.6	13	2	5.0	0.8
<i>Kuro-shima</i>					
V	–	24	14 ^a	3.1	1.8
H _q	–	44	35 ^b	5.6	4.5
H _t	–	27	19 ^b	3.5	2.4
Amorphous	–	61	0	7.8	0.0
Total	7.8	156	68	20.0	8.7

^a Kogure and Matsukura (2012a).

^b Kogure and Matsukura (2010a).

likely destabilized by notch development and occurs at risk for collapse toward the sea. Therefore, the crack is likely a tension crack generated in the horizontal failure surface. Table 3 lists the results of the measurements at T2, T3 and T5 and B1–B2 in Taketomi-jima. The dimensions of T2, T3 and T5 are as follows: $L = 1.3\text{--}5.9$ m; $\beta L = 0.9\text{--}4.3$ m ($\beta = 0.72\text{--}0.81$); $b = 2.4\text{--}2.5$ m; $H = 0.9\text{--}2.3$ m; and $h = 0.6\text{--}0.7$ m. The length of the horizontal tension crack at T3 is 0.8 m, which corresponds to 50% of the length of the potential failure surface.

4.2. Stability analysis

The β_{pred} value was calculated for T2, T3 and T5 by substituting their corresponding parameters into Eq. (4). The results indicated that the current notch depth at T2, T3 and T5 equals that required for collapse because β_{meas} , which is the β value measured in the field investigation, was 0.81 for T2, 0.73 for T3 and 0.72 for T5, while β_{pred} was 0.81, 0.79 and 0.79, respectively (Table 3).

Through investigations in Kuro-shima, Kogure and Matsukura (2010a) compared the β_{meas} and β_{pred} values for H_q-type collapses to determine whether the notch depth at collapse was large enough to facilitate gravity-induced collapse. Based on their results, as shown in Fig. 10, they claimed that the data plotted along the $\beta_{\text{meas}} = \beta_{\text{pred}}$ line are surely derived from gravitational collapse. The errors between β_{meas} and β_{pred} were below 0.1 for 65% of the blocks. However, these errors widely ranged from 0 to 0.66 (Kogure and Matsukura, 2010a). Kogure and Matsukura (2010a) recognized that their equations generate the correct β_{pred} value with an error of not more than 20% because the data plotted above the $\beta_{\text{meas}} = \beta_{\text{pred}}$ line satisfy $\beta_{\text{meas}}/\beta_{\text{pred}} < 1.2$, as shown with a shaded area in Fig. 10. Kogure and Matsukura (2010b) confirmed that almost all the blocks plotted outside the shaded area are not produced by gravitational collapses but by wave-induced collapses through stability analysis considering the wave pressure. Therefore, the lower limit of the shaded area likely indicates the border between gravity- and wave-induced collapses. This supports the correctness of the model proposed by Kogure and Matsukura (2010a).

The β_{meas} and β_{pred} values at T2, T3 and T5 are shown in Fig. 10 together with data obtained from Kogure and Matsukura (2010a). All of the data pertaining to T2, T3 and T5 are close to $\beta_{\text{meas}} = \beta_{\text{pred}}$ line, suggesting that the cliffs are ready to collapse at any moment. Considering that T3 contains a horizontal tension crack with a length that is half of that of the potential failure surface, the cliff stability has likely been greatly reduced. Therefore, the appearance of a stable cliff, i.e., T3, may

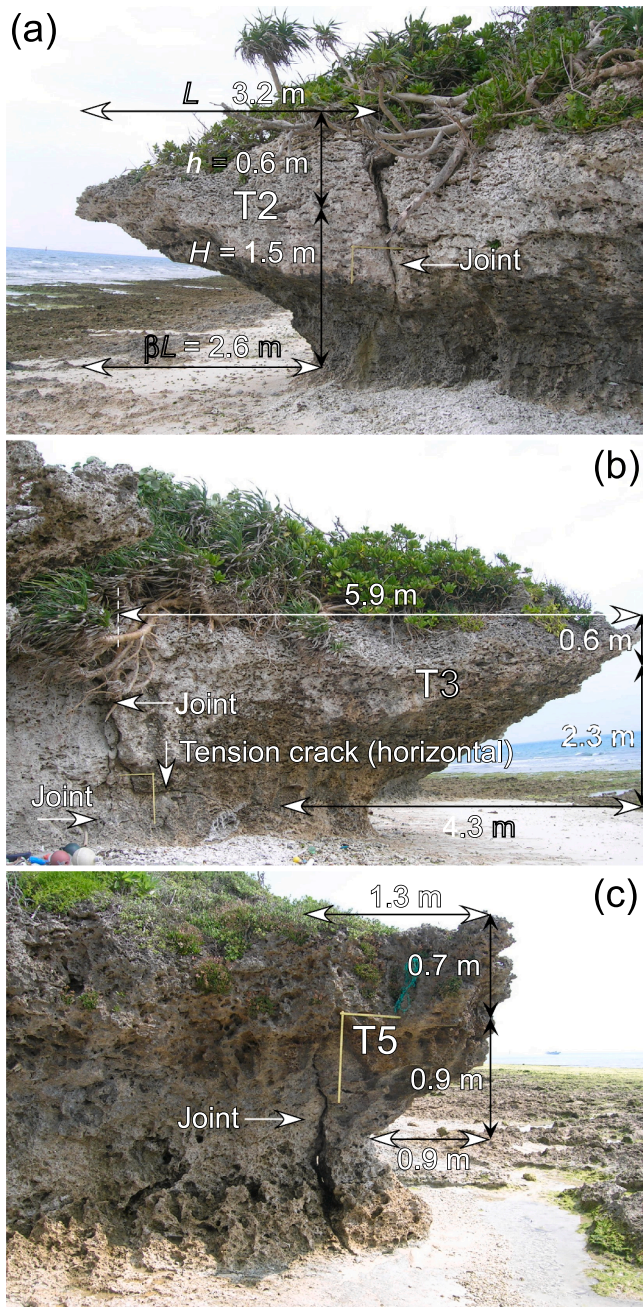


Fig. 9. Photos showing the dimensions of the coastal cliffs in Taketomi-jima considered in stability analysis: (a) T2; (b) T3; (c) T5.

Table 3
Dimensions of coastal cliffs and fallen blocks in Taketomi-jima.

No.	Type	L m	βL m	β_{meas}	b m	H m	h m	β_{pred}^a
<i>Cliff</i>								
T2	H _q	3.2	2.6	0.81	2.4	1.5	0.6	0.8
T3	H _q	5.9	4.3	0.73	2.5	2.3	0.6	0.8
T5	H _q	1.3	0.9	0.72	2.5	0.9	0.7	0.8
<i>Fallen block</i>								
B1	V	1.8	–	–	3.0	0.7	0.8	–
B2	V	3.1	–	–	2.7	1.1	0.7	–

^a The value was calculated by Equation (4).

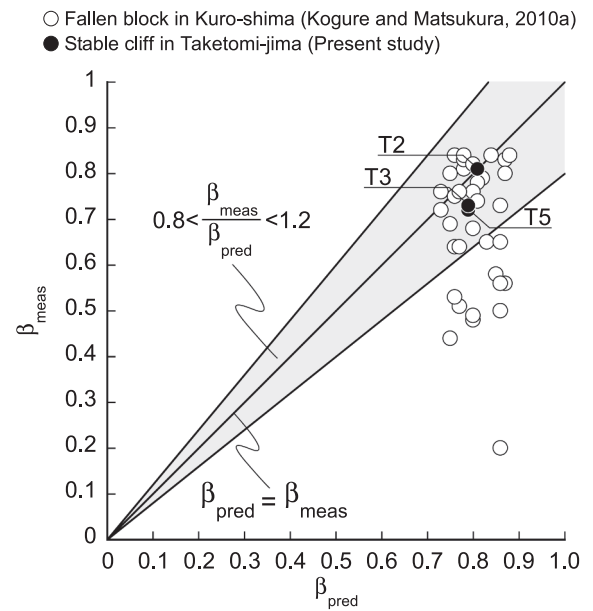


Fig. 10. Results of stability analysis. The open circles plotted outside of the shaded area indicate the cliffs collapsed by extreme waves such as tsunamis (Kogure and Matsukura, 2010b).

be attributed to reinforcement by PO roots. This situation is consistent with the fact that no horizontal tension cracks occur in the notched face of the cliffs in Kuro-shima where no PO grows on the top surface of the cliffs just above the notches (Fig. 5).

5. Discussions

The difference in vegetation occurrence between the coastal cliffs in Taketomi-jima and Kuro-shima and the stability analysis results indicate that the cliffs in Taketomi-jima are reinforced by the PO root system. The feasibility of reinforcement is discussed below in addition to the factors differentiating the occurrence of vegetation on the cliffs and prospects of future changes in the cliff collapse frequency caused by SLR.

5.1. Reinforcement of coastal cliffs by tree root systems

The stability analysis results indicate that the PO root system likely reinforces T2, T3 and T5 because these cliffs are unstable in terms of their dimensions (Fig. 10). PO develops a complex aerial root structure that provides additional stiffness and increases the drag coefficient against tsunami flow (e.g. Tanaka et al., 2007). However, to the author's knowledge, no reports have demonstrated or examined the root tensile strength (RTS) of PO. RTS measurement of PO may be difficult because the maximum root diameter is too large to conduct mechanical tests: the maximum root diameter is larger than 35 mm in males and 45 mm in females (Adkar and Bhaskar, 2014). Therefore, no data or equations are currently available to calculate the RTS of PO.

The mechanical properties of roots, including the RTS, have been reported for various kinds of shrubs and trees, although no data are available for PO. For example, the RTS of cedar has been measured in many studies to evaluate the effects of tree roots on slope stability (e.g. Genet et al., 2008). Genet et al. (2008) measured the RTS of 30-year-old cedar trees with a diameter ranging from 0.30 – 4.30 mm under a deformation rate of 10 mm/min and reported a mean strength of 31.7 MPa. Leung et al. (2015) measured the RTS of four types of native shrubs and trees in Hong Kong with diameters of 0.4–15.8 mm and reported that the RTS values, ranging from 3.3 to 345.1 MPa, were on the same order as the RTS values reported by Abdi et al. (2010), Burylo et al. (2011), De Baets et al. (2008), Ji et al. (2012) and Vergani et al. (2012)

for shrub and tree species in the Mediterranean, Iran, Alps of France, China and Italian Alps, respectively. These measurements demonstrate that the tensile strength of these shrub and tree roots is, at most, two orders of magnitude larger than that of Ryukyu limestone reported by Kogure (2009) (Table 1). Assuming that the RTS of PO is on the same order as that of the other shrub and tree species mentioned above, the PO roots densely growing on the cliff surface in Taketomi-jima can significantly increase the cliff stability.

5.2. Differentiating factors for the occurrence of vegetation on the cliffs

Although PO is a plant that is highly salt and wind tolerant, it may experience moderate to severe salt and wind damage during severe storms and hurricanes (Bezona et al., 2001). Similar extreme climatic events also occur in the Ryukyu Islands. The Ryukyu Islands are located in a subtropical area, and in summer and autumn, typhoons often pass across the islands. These events give rise to bores attributed to extreme waves in the Ryukyu Islands. Severe damage to the coastal environment due to bores has been reported since the late 1980 s (e.g. Nakaza et al., 1988). As shown in Fig. 11, a large amount of upward spray with a higher elevation than that of the cliff (4–5 m) occurs as a result of wave compaction at a cliff face. Consequently, the coastal cliffs in Taketomi-jima and Kuro-shima, with heights that are similar to those of the cliffs introduced in Nakaza et al. (1988), can also suffer from extreme waves during strong typhoons (Kogure and Matsukura, 2010b), which can result in severe damage to PO.

Fig. 11 suggests that the relationship between the wave height and cliff height can control the spray amount, which transports salt to PO growing on the top surface of the cliffs. Therefore, the occurrence of PO on the coastal cliffs in Taketomi-jima and Kuro-shima may also be controlled by the difference in cliff elevation between these islands. Kawana (1987) reported that the sea level around both islands remained constant for ca. 3000 years from ca. 4000 to 1000 years ago and that the island elevation increased due to seismic activity over the last 1000 years. The occurrence of relative uplift is evidenced by the higher altitude of the retreat point of the notches on the islands than the mean sea level (Fig. 8) because the notch retreat point is usually formed at the mean sea level (Focke, 1978). Therefore, it is plausible that the difference in uplift amount between these islands, which is estimated as ca. 1 m (Fig. 8), has occurred over the last 1000 years, although the cause of the difference remains unclear.

A substantial amount of sea spray reaches the cliff top surface just above a given notch upon wave impact during a severe storm or typhoon (Fig. 11). This is more likely to occur in Kuro-shima, where the cliff top surface elevation is ca. 1 m lower (Fig. 8). Therefore, it is clear that wave impact-related sea spray occurs more abundantly on the cliff top surfaces in Kuro-shima than in Taketomi-jima, which can result in the disappearance of PO through the supply of salt.

5.3. Possible increase in cliff collapses caused by future SLR

The apparent frequency of fallen blocks with source cliffs in Taketomi-jima is approximately one tenth of that in Kuro-shima currently (Table 2). The difference in apparent frequency between these islands indicates that many coastal cliffs in Taketomi-jima can be protected by PO growing on the top surfaces, such as T2, T3 and T5. Protection by PO is likely to be achieved by the higher elevation in Taketomi-jima than that in Kuro-shima by ca. 1 m as discussed above. Horton et al. (2020) reported global SLR projections with two uncertainty ranges and a median estimate under the two temperature scenarios of Representative Concentration Pathways (RCPs) 2.6 (which limits warming to 1 °C by 2100 and 1.2 °C by 2300 relative to 1986–2005) and 8.5 (which limits warming to 4.5 °C by 2100 and 12.6 °C in 2300 relative to 1986–2005), as defined in the Intergovernmental Panel on Climate Change (IPCC) Fifth Assessment Report (AR5). Under RCP2.6, the results suggest a likely SLR range (17th to 83rd

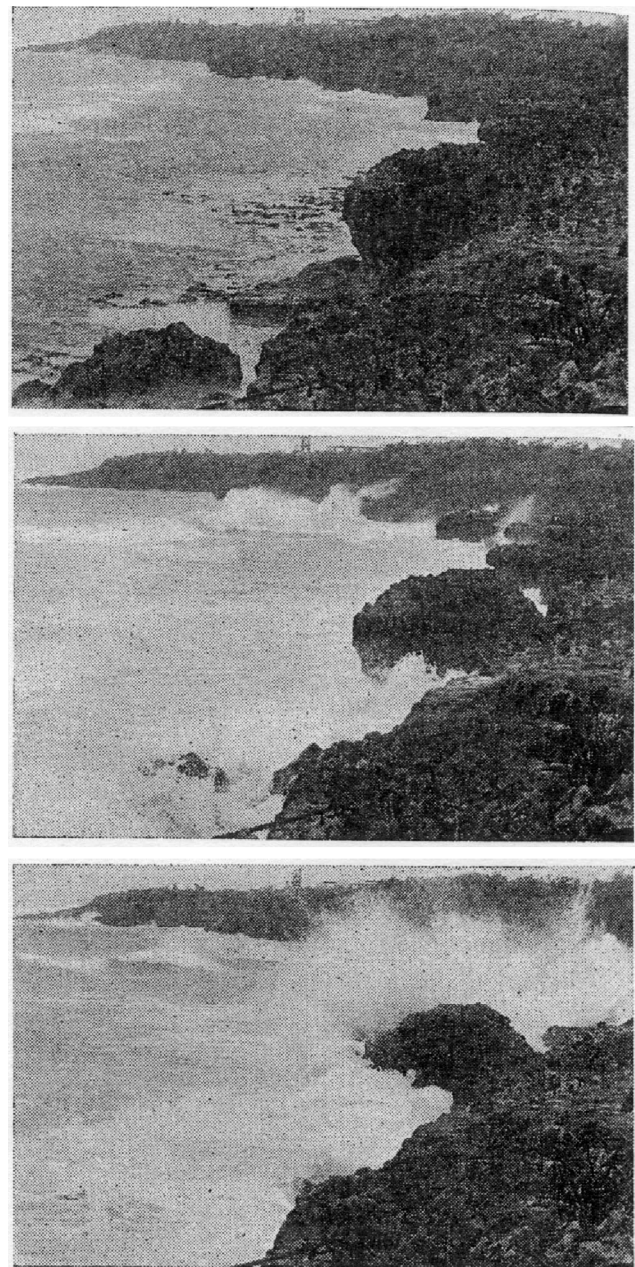


Fig. 11. Photographs of surging bores (Nakaza et al., 1988). Surging bores with a height ranging from 4 to 5 m and a period ranging from 10 to 15 min when a strong typhoon passes near the Ryukyu Islands.

Table 4

Ranges of global mean sea-level rise for 2100 and 2300 (modified after Table 1 in Horton et al. (2020)).

Year	Scenario	Likely range (m) (17th to 83rd percentiles)	Median (m) (50th percentile)	Very likely range (m) (5th to 95th percentiles)
2100	Lower (RCP 2.6)	0.30–0.65	0.45	0.21–0.82
	Upper (RCP 8.5)	0.63–1.32	0.93	0.45–1.65
2300	Lower (RCP 2.6)	0.54–2.15	1.18	0.24–3.11
	Upper (RCP 8.5)	1.67–5.61	3.29	0.88–7.83

percentiles) of 0.54–2.15 m, a very likely SLR range (5th to 95th percentiles) of 0.24–3.11 m, and a median of 1.18 m by 2300 (Table 4). Under RCP8.5, the likely SLR range is 0.63–1.32 m, the very likely SLR range is 0.45–1.65 m, and the median SLR value is 0.93 m by 2100 (Table 4). Therefore, an SLR of 1 m will be achieved by 2100 at the earliest and by 2300 at the latest. The future increase in SLR by 1 m will result in a similar relationship between the sea level and cliff top surface in Taketomi-jima to the present relationship in Kuro-shima. A change in the relationship will result in the disappearance of PO along the seaward edge of the cliff top surfaces in Taketomi-jima. PO disappearance will lead to the actual collapse of some cliffs, which should have already collapsed if they had not been reinforced by roots. Consequently, the possible disappearance of PO in Taketomi-jima caused by an SLR of 1 m over the following several decades or hundreds of years can increase the apparent frequency of block collapse with source cliffs by tenfold, similar to the present condition in Kuro-shima.

Fig. 3 shows that PO widely grows in coastal areas in tropical and subtropical regions. PO disappearance related to SLR could also occur on the low-lying coastal cliffs in these areas. Thus, this could also result in an increase in the apparent frequency of cliff collapses, especially for cliffs with a top surface elevation below 5 m, similar to those discussed in this study.

6. Conclusions

Stability analysis was conducted for the coastal cliffs in Taketomi-jima, Okinawa, Japan, to evaluate the effect of the aerial root system of PO on cliff stability. The results were compared to those reported for Kuro-shima, a neighboring island with similar environmental conditions. The concluding remarks obtained in this study are:

- The coastal cliff elevation is higher in Taketomi-jima than that in Kuro-shima by approximately 1 m, which results in the presence of PO on the seaward edge of the coastal cliffs in Taketomi-jima and in its absence in Kuro-shima;
- The root system of PO likely reinforces some of the cliffs in Taketomi-jima because the stability analysis results indicate that these cliffs are unstable in terms of their dimensions;
- Possible PO disappearance in Taketomi-jima caused by a SLR of 1 m over the following several decades or hundred years can increase the apparent frequency of cliff collapses by approximately tenfold.

Declaration of Competing Interest

The authors declare that they have no known competing financial interests or personal relationships that could have appeared to influence the work reported in this paper.

Acknowledgements

This study was partly supported by JSPS KAKENHI Grant Number JP21H01593 and JP21K18794.

References

- Abdi, E., Majnounian, B., Genet, M., Rahimi, H., 2010. Quantifying the effects of root reinforcement of Persian ironwood (*Parrotia persica*) on slope stability; a case study: hillslope of Hyrcanian forests, northern Iran. *Ecol. Eng.* 36, 1409–1416. <https://doi.org/10.1016/j.ecoleng.2010.06.020>.
- Adkar, P.P., Bhaskar, V.H., 2014. *Pandanus odoratissimus* (Kewda): a review on ethnopharmacology, phytochemistry, and nutritional aspects. *Adv. Pharmacol. Sci.* 1–19. <https://doi.org/10.1155/2014/120895>.
- Alongi, D.M., 2008. Mangrove forests: Resilience, protection from tsunamis, and responses to global climate change. *Estuar. Coast. Shelf Sci.* 76, 1–13. <https://doi.org/10.1016/j.ecss.2007.08.024>.
- Bezona, N., Hensley, D., Yogi, J., Tavares, J., Rauch, F., Iwata, R., Kellison, M., Wong, M., 2001. Salt and Wind Tolerance of Landscape Plants for Hawaii. Cooperative Extension Service, College of Tropical Agric. Human Reso., Univ. Hawaii at Manoa. *Landscape L-13*.
- Bruun, P., 1962. Sea level rise as a cause of shore erosion. *Journal of Waterways Harbour Division* 88, 117–130. <https://doi.org/10.1061/JWHEAU.0000252>.
- Burylo, M., Hudek, C., Rey, F., 2011. Soil reinforcement by the roots of six dominant species on eroded mountainous marly slopes (Southern Alps, France). *Catena* 84, 70–78. <https://doi.org/10.1016/j.catena.2010.09.007>.
- Callmänder, M.W., Gallaher, T.J., McNeill, J., Beentje, H., Nadaf, A.B., Middleton, D.J., Buerki, S., 2021. Neotypification of *Pandanus odorifer*, the correct name for *P. odoratissimus* (Pandanaeae). *Taxon* 70, 182–184. <https://doi.org/10.1002/tax.12406>.
- Davies, P., Williams, A.T., Bomboe, P., 1991. Numerical modelling of Lower Lias rock failures in the coastal cliffs of South Wales. In: Kraus, N.C., Gingerlich, K., Kreibel, D. L. (Eds.), *Coastal Sediments '91*. ASCE, New York, pp. 1599–1612.
- De Baets, S., Poesen, J., Reubens, B., Wemans, K., De Baerdemaeker, J., Muys, B., 2008. Root tensile strength and root distribution of typical Mediterranean plant species and their contribution to soil shear strength. *Plant Soil* 305, 207–222. <https://doi.org/10.1007/s11104-008-9553-0>.
- Discover Life, 2021. *Pandanus Odoratissimus*. <https://www.discoverlife.org/mp/20q?search=Pandanus+odoratissimus> (accessed 11 May 2021).
- Focke, J.W., 1978. Limestone cliff morphology and organism distribution on Curaçao (Netherlands Antilles). *Leidsche Geol. Meded.* 51, 131–150.
- Genet, M., Kokutse, N., Stokes, A., Fourcaud, T., Cai, X.H., Ji, J.N., Mickovski, S., 2008. Root reinforcement in plantations of *Cryptomeria japonica* D. Don: effect of tree age and stand structure on slope stability. *For. Ecol. Manage.* 256, 1517–1526. <https://doi.org/10.1016/j.foreco.2008.05.050>.
- Geospatial Information Authority of Japan, 2021. Elevation - Global version. <https://globalmaps.github.io/el.html> (accessed 10 May 2021).
- Hay, C.C., Morrow, E., Kopp, R.E., Mitrovica, J.X., 2015. Probabilistic reanalysis of twentieth-century sea-level rise. *Nature* 517, 481–484. <https://doi.org/10.1038/nature14093>.
- Horton, B.P., Khan, N.S., Cahill, N., Lee, J.S.H., Shaw, T.A., Garner, A.J., Kemp, A.C., Engelhart, S.E., Rahmstorf, S., 2020. Estimating global mean sea-level rise and its uncertainties by 2100 and 2300 from an expert survey. *npj Clim. Atmos. Sci.* 3, 18. <https://doi.org/10.1038/s41612-020-0121-5>.
- Hutchinson, J.N., 1972. Field and laboratory studies of a fall in upper chalk cliffs at Joss Bay, Isle of Thanet. *Proceedings of the Roscoe Memorial Symposium*. G.T. Foulis & Co. Ltd., Cambridge, pp. 692–706.
- Ji, J., Kokutse, N., Genet, M., Fourcaud, T., Zhang, Z., 2012. Effect of spatial variation of tree root characteristics on slope stability. A case study on black locust (*Robinia pseudoacacia*) and arborvitae (*Platycladus orientalis*) stands on the loess plateau. *China. Catena* 92, 139–154. <https://doi.org/10.1016/j.catena.2011.12.008>.
- Kathiresan, K., Rajendran, N., 2005. Coastal mangrove forests mitigated tsunami. *Estuar. Coast. Shelf Sci.* 65, 601–606. <https://doi.org/10.1016/j.ecss.2005.06.022>.
- Kawana, T., 1987. Holocene diastrophism around the Sekisei lagoon in Okinawa. *Earth Mon. J.* 9, 129–134 in Japanese.
- Kogure, T., 2009. Physical and Mechanical Properties of Ryukyu Limestone in Kuro-shima and Taketomi-jima in Yaeyama Islands, Okinawa, Japan. *Bull. Terr. Environ. Research Center. Univ. Tsukuba* 10, 61–67 in Japanese.
- Kogure, T., Aoki, H., Maekado, A., Hirose, T., Matsukura, Y., 2006. Effect of the development of notches and tension cracks on instability of limestone coastal cliffs in the Ryukyus. *Japan. Geomorph.* 80, 236–244. <https://doi.org/10.1016/j.geomorph.2006.02.012>.
- Kogure, T., Matsukura, Y., 2010a. Critical notch depths for failure of coastal limestone cliffs: case study at Kuro-shima Island, Okinawa. *Japan. Earth Surf. Process. Landf.* 35, 1044–1056. <https://doi.org/10.1002/esp.1940>.
- Kogure, T., Matsukura, Y., 2010b. Instability of coral limestone cliffs due to extreme waves. *Earth Surf. Process. Landf.* 35, 1357–1367. <https://doi.org/10.1002/esp.2046>.
- Kogure, T., Matsukura, Y., 2011. Effect of vertical joints on the planar shape of fallen blocks in coastal cliff collapses at Kuro-shima, Okinawa. *Japan. Trans. JGU.* 32, 15–28.
- Kogure, T., Matsukura, Y., 2012. Threshold height of coastal cliffs for collapse due to tsunami: Theoretical analysis of the coral limestone cliffs of the Ryukyu Islands. *Japan. Mar. Geol.* 323, 14–23. <https://doi.org/10.1016/j.margeo.2012.07.014>.
- Leatherman, S.P., Zhang, K., Douglas, B.C., 2000. Sea level rise shown to drive coastal erosion. *EOS, Trans. AGU.* 81 (6), 55–57.
- Letortu, P., Costa, S., Maquaire, O., Davidson, R., 2019. Marine and subaerial controls of coastal chalk cliff erosion in Normandy (France) based on a 7-year laser scanner monitoring. *Geomorph.* 335, 76–91. <https://doi.org/10.1016/j.geomorph.2019.03.005>.
- Leung, F.T., Yan, W., Hau, B.C., Tham, L., 2015. Root systems of native shrubs and trees in Hong Kong and their effects on enhancing slope stability. *Catena* 125, 102–110. <https://doi.org/10.1016/j.catena.2014.10.018>.
- Luijendijk, A., Hagenaars, G., Ranasinghe, R., Baart, F., Donchyts, G., Aarninkhof, S., 2018. State of the World's Beaches. *Sci. Rep.* 8, 6641. <https://doi.org/10.1038/s41598-018-24630-6>.
- Matsukura, Y., 2001. Rockfall at Toyohama Tunnel, Japan, in 1996: effect of notch growth on instability of a coastal cliff. *Bull. Eng. Geol. Environ.* 60, 285–289. <https://doi.org/10.1007/s100640100123>.
- Mazda, Y., Magi, M., Kogo, M., Hong, P.N., 1997. Mangrove on coastal protection from waves in the Tong King Delta. *Vietnam. Mangr. Salt Marsh.* 1, 127–135. <https://doi.org/10.1023/A:1009928003700>.
- Nakaza, E., Tsukayama, M., Hino, M., Ohosiro, T., 1988. A study on wave forces induced by wave groups. *Proc. 35th Jpn. Coast. Eng. Conf.* 597–601 in Japanese.
- Paling, E.I., Kobryn, H.T., Humphreys, G., 2008. Assessing the extent of mangrove change caused by Cyclone Vance in the eastern Exmouth Gulf, northwestern

- Australia. *Estuar. Coast. Shelf Sci.* 77, 603–613. <https://doi.org/10.1016/j.ecss.2007.10.019>.
- Sunamura, T., 1992. *Geomorphology of Rocky Coasts*. John Wiley & Sons, Chichester.
- Tanaka, N., Sasaki, Y., Mowjood, M.I.M., Jinadasa, K.B.S.N., Homchuen, S., 2007. Coastal vegetation structures and their functions in tsunami protection: experience of the recent Indian Ocean tsunami. *Landsc. Ecol. Eng.* 3, 33–45. <https://doi.org/10.1007/s11355-006-0013-9>.
- Vergani, C., Chiaradia, E., Bischetti, G., 2012. Variability in the tensile resistance of roots in Alpine forest tree species. *Ecol. Eng.* 46, 43–56. <https://doi.org/10.1016/j.ecoleng.2012.04.036>.
- Walsh, K.J., McBride, J.L., Klotzbach, P.J., Balachandran, S., Camargo, S.J., Holland, G., Knutson, T.R., Kossin, J.P., Lee, T.C., Sobel, A., Sugi, M., 2016. Tropical cyclones and climate change. *Wiley Interdiscip. Rev.-Clim. Chang.* 7, 65–89. <https://doi.org/10.1002/wcc.371>.
- Williams, A.T., Davis, P., Bomboe, P., 1993. Geometrical simulation studies of coastal cliff failures in liassic strata, South Wales. *UK. Earth Surf. Process. Landf.* 18, 703–720. <https://doi.org/10.1002/esp.3290180805>.
- Young, A.P., Carilli, J.E., 2019. Global distribution of coastal cliffs. *Earth Surf. Process. Landf.* 44, 1309–1316. <https://doi.org/10.1002/esp.4574>.
- Zhang, K., Douglas, B.C., Leatherman, S.P., 2004. Global warming and coastal erosion. *Clim. change* 64, 41–58. <https://doi.org/10.1023/B:CLIM.0000024690.32682.48>.